ELSEVIER

Diamond and Related Materials 7 (1998) 1605–1616

DIAMOND AND RELATED MATERIALS

Hollow cathode synthesis of crystalline CN films

Stephen Muhl *, Adriana Gaona-Couto, Gonzalo Gonzalez, Juan Manuel Méndez

Instituto de Investigaciones en Materiales, Universidad Nacional Autonoma de Mexico, Apartado Postal 70-360, Coyoacan, Mexico DF, 04510, Mexico

Received 29 October 1996; accepted 2 March 1998

Abstract

We describe a novel carbon hollow-cathode RF plasma reactor which has been used to prepare deposits of carbon nitride. Results of the characterization of the deposits by Fourier transform infrared (FTIR) microscopy, Raman microscopy, transmission electron microscopy (TEM), energy-dispersive X-ray analysis and X-ray diffraction are presented. The variation of the properties of the deposits as a function of the deposition conditions is discussed. The inclusion of small quantities of methane in the gas mixture was found to enhance the formation of the CN deposit, but for conditions of maximum enhancement C–H and N–H groups were observed in the deposit. Elemental analysis of the deposit showed that the nitrogen content was $\sim$57 at.%. A crystalline deposit was obtainable at low substrate temperatures, and the crystals were seen to grow preferentially on defects on the substrate surface. © 1998 Elsevier Science S.A. All rights reserved.

Keywords: Carbon nitride; Infrared spectroscopy; Morphology; Plasma-enhanced CVD

1. Introduction

The calculations of Liu and Cohen [1–4] predicting the exceptional properties of crystalline carbon nitride (CN) have been the stimulus for a great number of attempts to prepare this material. These attempts have involved a wide variety of methods, including sputtering a carbon target in a nitrogen atmosphere [5], laser ablation of graphite [6], pyrolytic decomposition of C–H–N organics [7], electron cyclotron resonance plasma chemical vapour deposition (CVD) [8], and low-energy nitrogen ion implantation in carbon [9]. However, the majority of the work has resulted in deposits with nitrogen concentrations below $\leq$40 at.%., which is substantially less than that of the stoichiometric value of $\sim$57 at.%. Some of the latest work using arc plasma-jet CVD, where the carbon source is a graphite anode [10], and laser ablation of a graphite rod with simultaneous N^+ ion bombardment [11], has reported nitrogen compositions near that of C_3N_4. The purpose of this paper is to report the preparation of crystallites of CN by a high power-density physical/chemical sputtering technique assisted by ion bombardment.

2. Experimental

The reaction chamber consisted of a rectangular stainless-steel box (40 cm × 40 cm × 20 cm), as shown schematically in Fig. 1(a). A detailed drawing of the water cooled electrode assembly is given in Fig. 1(b). The replaceable electrode insert exposed to the plasma (internal volume $\sim$3.5 cm^3) was made of dense, nuclear-grade graphite. The gases were introduced through the centre of the electrode and thereby through the graphite insert. The gas flows were regulated using MKS mass flow controllers, 100 sccm full scale for nitrogen (99.999% purity) and 10 sccm full scale for methane (99.999% purity). The gas pressure was measured by an MKS capacitance manometer, and this, together with an MKS variable throttle valve mounted on the inlet to the mechanical vacuum pump, controlled the chamber pressure. The chamber was equipped with various electrical and motion feedthroughs for the substrate heater supply, the substrate temperature measurement, the substrate bias, connection to the electrical plasma probe, the shutter and the vertical displacement of the electrical probe. The majority of the experiments were carried out using 1 cm × 1 cm pieces cut from high-resistivity silicon wafers. A selection of deposits were prepared on single-crystal graphite for ion-beam analysis work. Some experiments were also attempted using

* Corresponding author. Fax: +52 56161251;
e-mail: jmmendez@sunrise.ccs.yorku.ca

0925-9635/98/$ – see front matter © 1998 Elsevier Science S.A. All rights reserved.
PII S0925-9635(98)00168-X

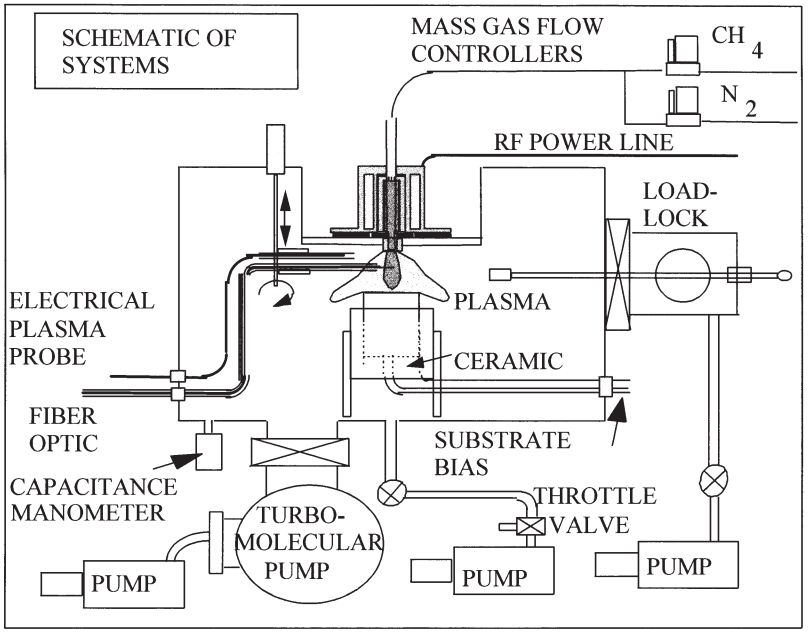

(a)

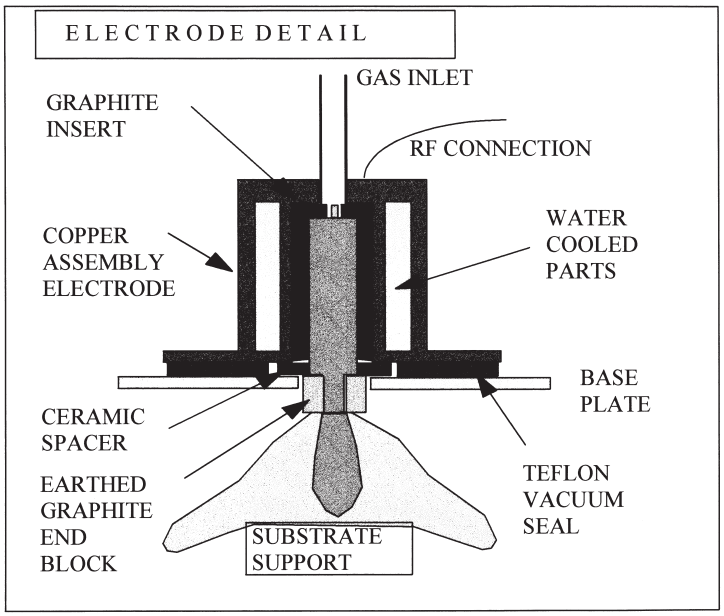

(b)

Fig. 1. (a) Schematic drawing of the reaction chamber. (b) Detail of the electrode assembly.

Electrode–substrate distance	1 cm
Gas pressure	0.5 Torr
Substrate temperature	100–200 °C (plasma heating)
Substrate bias	0– −300 V
RF plasma power	20–600 W
Deposition time	30–300 min
Gas flows	N_2, 40 sccm; CH_4, 0.75 sccm

sapphire and sodium chloride substrates: however, the deposition rate of the former was very low and the latter type was severely attacked by the plasma. Table 1 shows the experimental conditions used in this study. Basically, the characteristics of the deposits were determined as a function of the deposition time, the plasma power and the substrate bias. It should be noted that the plasma power density is very high, varying from 56 to 170 W cm^{-3}.

The reaction chamber was pumped down to $\sim 2 \times 10^{-6}$ Torr prior to the introduction of the reaction gases. An ENI 1 kW power supply together with a manual matching network and a Bird RF power meter were used to provide and measure the 13.56 MHz radio frequency power for the plasma generation. The samples

were analysed using Nicolet 205 and 510P Fourier transform infrared (FTIR) spectrophotometers (the latter has an IR microscope for small area analysis), a Dilor Micro-Raman probe using 632 nm laser light as the excitation signal, a Sloan Dektak IIA perfilometer, a Siemens D500 X-ray powder diffractometer using Cu Kα radiation, a Leica-Cambridge Stereoscan 440 scanning electron microscope equipped with an energy-dispersive X-ray analyser (EDX) for the elemental composition measurements, a JEOL JEM-1200EX transmission microscope for the electron diffraction, and finally, for the RBS measurements, a 2.0 MeV alpha-particle beam generated by the 5.5 MeV van de Graaff particle accelerator of the Instituto de Fisica of the National University of Mexico. The RBS spectra were analysed using the RUMP software developed by Cornell University [12]. The EDX elemental studies were calibrated using measurements of high-purity samples of melamine ($C_3N_6H_6$) and sodium cyanide (NaCN).

The Langmuir probe measurements involved the use of a 0.45 mm diameter tungsten wire, 6 mm in length, connected to a Keithley 237 Source/Measure unit interfaced to a 486 PC.

3. Results and discussion

Initially, experiments were performed using an electrode–substrate distance of ~5 cm, and very low deposition rates were obtained. The electrode–substrate distance was then reduced to ~1 cm, and this resulted in a considerable increase in the deposition rate. A gas pressure of 0.5 Torr was selected as a compromise between the possible tendency for an increase in the deposition rate with increasing pressure and the necessity to ensure that a plasma could not ignite inside the tubing supplying the gases to the electrode assembly at high pressures.

During these initial experiments, isolated columnar growth was observed by an optical microscope on the polished surface of the silicon substrates. The columns appeared to be associated with scratches in the substrate surface caused during cleaning and cutting. A significant increase in column growth was found for substrates which had had their surface abraded with fine silicon carbide powder. The abrasion of separate areas of a substrate with silicon carbide, tungsten carbide, boron nitride and mixtures of pairs of each, indicated that the existence of the columns depended on the degree of damage to the silicon and not on the inclusion of a particular material in the surface of the silicon. Given the difficulty of preparing identically abraded surfaces, the reverse matt back-surface of the pieces of silicon was used for subsequent runs.

Preliminary Langmuir probe studies of the plasma were carried out versus the plasma power (0.5 Torr, 40 sccm N_2, 0.75 sccm of CH_4 and no substrate bias). Subsequent analysis of the probe characteristics showed that the electron temperature, as measured ~2 mm above the substrate holder, increased from ~3 to 16 eV as the power was changed from 100 to 600 W. The corresponding change in the plasma potential was from 18 to 100 V. The plasma density was found to be $\sim 10^{10}$ cm^{-3} for all powers. These results indicate that the plasma contains electrons with sufficient energy to cause fragmentation of both the methane and nitrogen molecules [13,14], as well as sufficient energy to promote the formation, in the gas phase, of CN molecules [15].

Fig. 2 shows an area of the deposit with cone-shaped columns of material. The sample in this case was prepared on a silicon substrate with 40 and 0.75 sccm of N_2 and CH_4, respectively, at 0.5 T using 200 W RF power and a bias of −100 V. However, similar formations were found under most of the experimental conditions studied: only the number and size of the columns were seen to vary. Between the columns, much smaller sharp peaks of deposit can be observed. Additionally, in some areas larger more rectangular features can be seen. The observation of a columnar structure in the deposit generated the following questions:

(1) are the columns and the thinner under-layer of the same composition?;
(2) are the columns crystalline?; and
(3) how does the growth of these features vary with the experimental parameters?

In relation to question 1, the topography of the deposits severely limits the usefulness of the RBS technique. With this method, the beam diameter is such that areas with and without columns are analysed simultaneously, and since the perfilometer measurements show that the columns can be very high (up to ~10 μm), backscattering from the columns gives signals from both carbon and nitrogen, whilst for the intercolumnar areas the incident alphas penetrate through to the carbon substrate used for this study, resulting in an artificially high carbon signal in the final spectra. Indeed, the C/N ratios of the three samples analysed using this technique were all greater than unity. However, the RBS analysis did show that the deposit does contain nitrogen and carbon and only trace amounts of other elements, and that only small amounts of oxygen are found, probably as a surface layer.

The EDX technique permitted analysis of both the columns and the intercolumnar areas of deposits prepared on silicon substrates. The analysis showed that both areas are of the same composition, and this did not seem to depend on the experimental variables within the ranges investigated. However, further work is required as only samples prepared as a function of plasma power (100–600 W) were studied, the other experimental conditions being 0.5 Torr, 40 sccm of N_2,

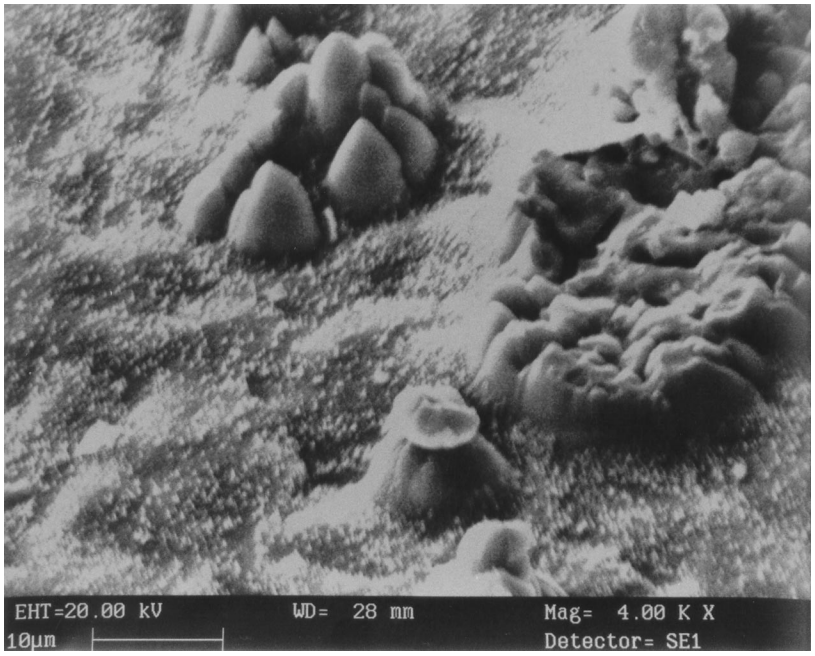

Fig. 2. Microphotograph of a typical area of the deposit surface.

0.75 sccm of CH_4 and a bias of -100 V. The EDX signal from the silicon substrate varied between the two areas studied because of the difference in the thickness of the deposit, and therefore the silicon signal was not included in the calculation of the composition. After calibration measurements with substances of known composition were performed, we found that the carbon-to-nitrogen ratio was 0.75 ± 0.03. This is the stoichiometric value for C_3N_4: however, because of interference from the substrate it was not possible to define the silicon content of the deposit.

The irregular surface of the deposits signified that meaningful thickness measurements of the samples by perfilometry were not possible. However, this technique did give useful information about the maximum height and number of columns in typical areas of the surface as a function of the deposition time. These results are presented in Fig. 3. The maximum column height was seen to remain almost unchanged for deposition times <120 min, and increased by a factor of 5 for 300 min, indicating that the growth process is not linear with time. It seems that the large columns become established and then dominate the growth process. As a function of the substrate bias, the height increased slowly from 2 to 4 µm as the bias changed from 0 to -300 V. The variation as a function of the plasma power is somewhat more complicated, and no clear trend was observed.

Thus, it appears that there is an initial nucleation stage for column growth after which large columns develop rapidly. This nucleation stage and the development appears to be affected by bombardment of the deposit by plasma species. The degree of substrate bombardment is principally controlled by the bias and the plasma potential, which in turn depends on the plasma power. However, given that the mean free path of the plasma species is of the order of 0.1 mm, the hollow cathode–substrate distance of 1 cm should mean that the species are thermalized before reaching the substrate, with this strongly reducing any bombardment affects due to ions and atoms. Under these conditions the substrate bias can only cause acceleration of the ions over a distance of a few times the mean free path without resulting in high-energy bombardment. Therefore, we feel that chemical sputtering is probably the principal mechanism which competes with the growth process, and this is why there is a complicated relationship between the existence of large columns and the plasma power and the substrate bias, since both of these affect the proportions of the various species generated in the plasma and their impingement rate on the growing film surface.

Electron diffraction measurement of areas of the samples containing the {100} crystalline silicon permitted calculation of the microscope constant, and this was used in the analysis of one of the sample diffraction patterns. Fig. 4 shows a typical incomplete ring diffraction pattern and bright-field image from a deposit. The reported and measured *d*-spacings are given in Table 2 [16,17]. A reasonable agreement between our data, that of other authors [10,18] and that reported for β-C_3N_4 can be seen, but the corresponding intensities are somewhat at variance and some *d*-spacings are not observed. From these diffraction results, we conclude that the deposit contains small crystallites ($\sim$100 nm). Furthermore, although the characteristic distances of the α and β hexagonal phases are very similar [19,20],

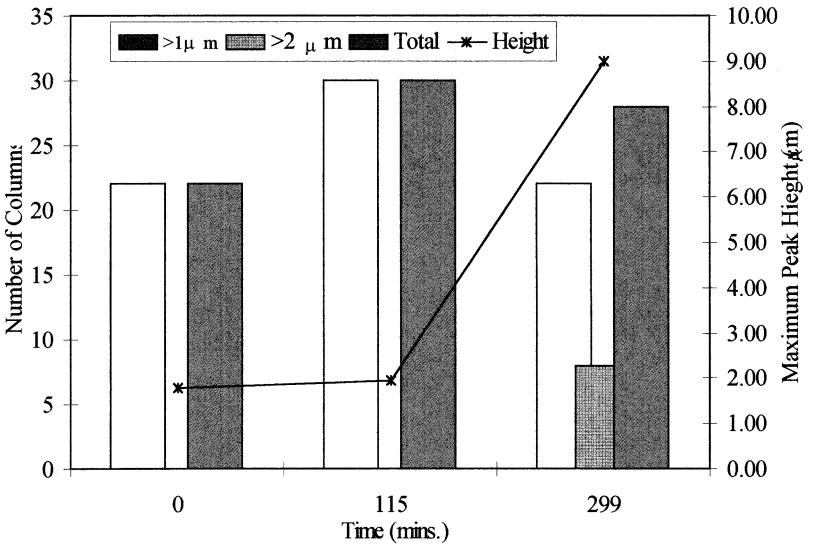

Fig. 3. Variation of the maximum column height and the distribution of the column height for a 1 mm scan as a function of the deposition time.

the α phase has planes near to 0.15 nm, and since these are not observed, this phase is not present. Similarly, the β cubic phase can be excluded by the absence of distances >0.22 nm, together with the existence of the 0.77 nm reflection. Similar comparisons can be carried out to rule out the presence of the pseudo-cubic and graphite phases. Therefore, it is possible that the deposit consists of crystallites of β-hexagonal C_3N_4.

X-ray diffraction studies showed the presence of various peaks other than those associated with the {100} silicon substrate. In particular fairly strong peaks were seen at values of 2θ of 66.0, 45.2 and 43.2°, with smaller peaks at 15.8, 28.5, 41.3, 48.7, 57.5 and 69.8°. These peaks correspond quite well with the 2θ values calculated for C_3N_4 using the crystal diffraction module of the Cerius2™ program developed by BIOSYM/Molecule Simulations. The results are presented in Table 3, together with the *d*-spacings and the relative intensities. The position of the peaks from this program can only be considered as approximate, as the model used is based on unstressed and perfectly relaxed crystallites. Similarly, the relative intensities are for randomly orientated microcrystals. Therefore, if as is often seen, the deposit grows with a preferred orientation, then the observed intensities will not coincide with the theoretical values. The intensities of the strong peaks were seen to increase with increasing plasma power and with the substrate bias, and the smaller peaks were only distinguishable at the highest powers and for times >100 min. These observations agree with the column distribution data presented earlier.

FTIR measurements were performed on samples deposited on silicon, and showed absorption bands at ~2200, 1530, 1210, 1000 and 800 cm^{-1}. The band at 2200 cm^{-1} corresponds to the C≡N stretching mode [21]. This bonding arrangement is not compatible with an extended inorganic solid, but may be in a surface layer, although it is possible that there is a contribution to this peak from Si–H bonds. The broad band observed at 1530 cm^{-1} has been related to either C=N [22], or to sp^2 carbon which has become IR-active through the incorporation of nitrogen into the graphite rings [23]. However, the incorporation of nitrogen normally means that the accompanying Raman-active D band at 1360 cm^{-1} should also be observed in the IR spectra, and this is not the case in our samples. The band at 1200 cm^{-1} is considered to be attributed to linear C–N stretching [24]. The assignment of the band at 830 cm^{-1} is difficult since there are known bands at ~780 cm^{-1} related to Si–C stretching, and triazine rings show a deformation peak in this region, but at slightly higher energies (i.e. 820–830 cm^{-1}). Absorption bands in this range have been reported, apparently related to structures having nitrogen bonded to three carbon atoms in a pyramidal arrangement [25]. Such bands are also obtained if Chen's scaling factor of 1.43 [10] is used to simulate the C_3N_4 spectra from that of β-Si_3N_4. Additionally, a peak at 826 cm^{-1} was observed in a hard material with a C_3N_4 composition [26]. Thus the 800 cm^{-1} peak may be related to a deformation mode of an as yet not well-defined structure containing C–N bonds. The absence of peaks at ~870–890 cm^{-1} indicates there is very little, if any, formation of Si–N. The peak near to 1000 cm^{-1} is also difficult to identify: single bonds such as C–N and =C–N are found in the 1020–1433 cm^{-1} and 1050–1490 cm^{-1} regions, respectively [27]. However, the 1000 cm^{-1} peak is not considered in the detailed analysis, since it is not clear that it corresponds to the type of bonding mentioned above, but may be related to a deformation mode which is distinct from that responsible for the 800 cm^{-1} band. Furthermore, recent theoretical work [28] shows that

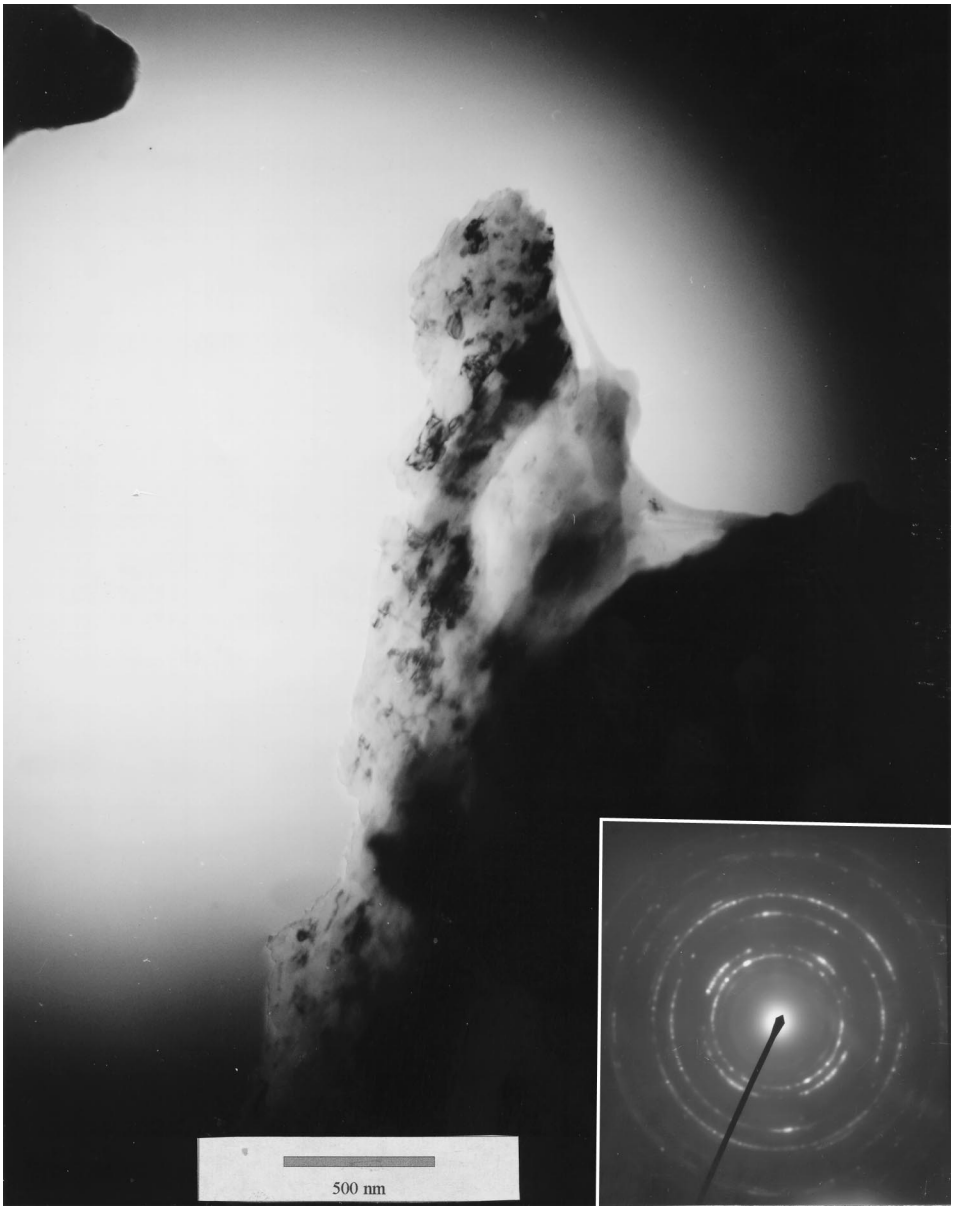

Fig. 4. Selected-area electron diffraction pattern and bright field image of a CN deposit prepared at 200 W, 40 sccm N_2, 0.75 sccm CH_4, 0.5 Torr and a bias of −200 V.

β-C_3N_4 should exhibit IR absorption in bands centred at ~1450, 1200, 800, 700 and 450 cm^{-1}, and that rhombohedral C_3N_4 gives bands at ~1750, 1580, 1200, 800, 700, 550 and 350 cm^{-1}. In summary, for the rest of this section we use the following band assignments: 2200 cm^{-1} as C≡N, 1530 cm^{-1} as C=N, and 800 and 1210 cm^{-1} as C–N.

Small-area FTIR permitted analysis of areas of the deposit with and without large columns. Fig. 5(a) and (b) show the IR absorption spectra of the base area and the column-containing areas of samples prepared at 500 W, 0.5 Torr, 40 sccm N_2 and 0.75 sccm CH_4 at deposition times of 60, 115 and 300 min. Small absorption bands can be seen at ~3350 and 2900 cm^{-1}, associated with N–H and C–H groups, respectively. However, the large absorption cross-sections of these bands implies that the hydrogen content of the deposits is very small. The data related to the carbon–nitrogen bonds provides useful information as to the growth and development of the deposit. Based on the single-, double- and triple-bond assignments assumed earlier, it can be seen that initially the deposit contains similar amounts of –N, =N and ≡N (assuming that the absorption cross-sections for the three bands are equal), with somewhat more in the area of the columns than in the base area. For a deposition time of 115 min, the amount of –N and ≡N increases greatly, the latter significantly more. For longer times, the ≡N content remains almost

Table 2
X-ray diffraction results and the Cerius2™ calculated values

$2-\theta$ (experimental)	$2-\theta$ (calculated)	d values	Intensity
15.8(w)	15.9	5.577	5.21
28.5(w)	27.7	3.220	36.00
	32.1	2.789	100.00
41.3(w)	40.0	2.253	61.58
43.2(s)	42.9	2.108	43.24
45.2(s)	46.4	1.956	60.84
48.7(w)	49.0	1.859	38.48
	49.4	1.846	0.07
	57.2	1.610	2.53
57.5(w)	57.5	1.601	11.42
	59.8	1.547	10.98
	62.6	1.484	11.41
66.0(s)	67.1	1.394	0.03
69.8(w)	69.8	1.348	16.03

The letters in parentheses indicates strong and weak peaks.

Table 3
Calculated and observed d-spacings and intensities for the electron diffraction

TEM d (A)	I	Theory d (A)	I	(hkl)
2.75	w	2.77	s	200
2.21	w	2.20	s	101
		2.09	s	210
1.92	s	1.92	m	111
		1.85	m	300
1.67	s	1.60	w	220
1.19	w	1.13	vw	401
1.01	w	1.03	vw	501
0.96	m	0.97	vw	430
0.83	m	0.85	vw	152
0.77	w	0.67	w	611
$a=6.52$ Å		6.40 Å		
$c=2.41$ Å		2.40 Å		

the same but the –N content continues to increase, the increase being larger for the base area, but in total the amount is still less than in the columns. It should be noted that in general, absorption in the column areas is greater than the base areas, indicating that there is more CN-containing material in the columns.

Fig. 6(a)–(d) shows in more detail the trends described above, i.e. the variation of the areas and centre positions of the 2200, 1500, 1200 and 800 cm^{-1} peaks as a function of the deposition time for both the base and column areas. In an attempt to remove the effects of variations in the measurement conditions, the raw data was divided by the value of the absorbance at 1950 cm^{-1}. This value was chosen because no bands or tails of bands were found around this wavenumber. The data for the different bands were obtained by fitting Gaussian functions to the appropriate parts of the normalized spectra. From Fig. 6(a), two trends can be seen. First, for the initial 120 min of deposition, the C≡N content increases in both the column and base areas, but for longer times the number of triple-bonded nitrogens decreases in the columns relative to the base area. Secondly, the band position moves to lower energies during the first 120 min, indicating changes in the environment of the triple bond. The dependence of C=N on the deposition time (Fig. 6(b)) for the column and base areas is qualitatively the same in that both decrease rapidly for <120 min and more slowly thereafter. However, the positions of the peaks vary in different ways: within the analysis error, the base-area peak position does not change, but the peak related to the columns moves to higher energies. As demonstrated by the 1200 and 800 cm^{-1} bands, the amount of C–N varies in different ways with the deposition time. For the first case, the area of the band for both the column and base areas increases rapidly for short times and more slowly thereafter. As in the previous case, the variation of the peak position is different for the two areas; the column-area peak moves slightly to higher energies, while the base-area peak moves to lower energies. The amount of 800 cm^{-1} C–N in the columns increases initially and saturates for deposition times >120 min. Similarly, the amount in the base area increases continually with deposition time. At first sight the results for the 1200 cm^{-1} band and the 800 cm^{-1} band appear to be somewhat contradictory. However, it should be noted that the 1200 cm^{-1} peak corresponds to a single carbon–nitrogen bond in a structure where the nitrogen is not necessarily bonded to a total of three carbon atoms, whilst the 800 cm^{-1} peak relates to the case where the nitrogen is bonded to three carbon atoms, which is possible at the apex of this group of atoms. The figures show that the difference between the column and base areas for all the peak areas and positions is smallest for a deposition time of 120 min. Unfortunately, this was the time chosen to study the variation of the peaks versus the plasma power and the substrate bias, and therefore no significant variation between the two areas was observable.

As either the plasma power was increased from 200 to 600 W (with a bias of -200 V), or the substrate bias was increased from 0 to -300 V (at a power of 500 W), the area and position of the 2200 cm^{-1} band decreased (the area by a factor of 10 and the position by ~ 20 cm^{-1}), and the area and position of the 800 cm^{-1} band increased (the area by a factor of 10 and the position by ~ 50 cm^{-1}). The area and position of the 1500 cm^{-1} peak decreases as the plasma power or substrate bias increases, and the peak virtually disappears for powers >400 W and biases >-150 V, possibly meaning that the graphitic phase is considerably decreased. The absorption of the nitrile group, when linked in a ⟩N–C≡N manner, is observed between 2175 and 2225 cm^{-1} [25], exactly as found in our samples. The shift to lower energies may be due to a change in the angle of the bonds of the left-hand side nitrogen

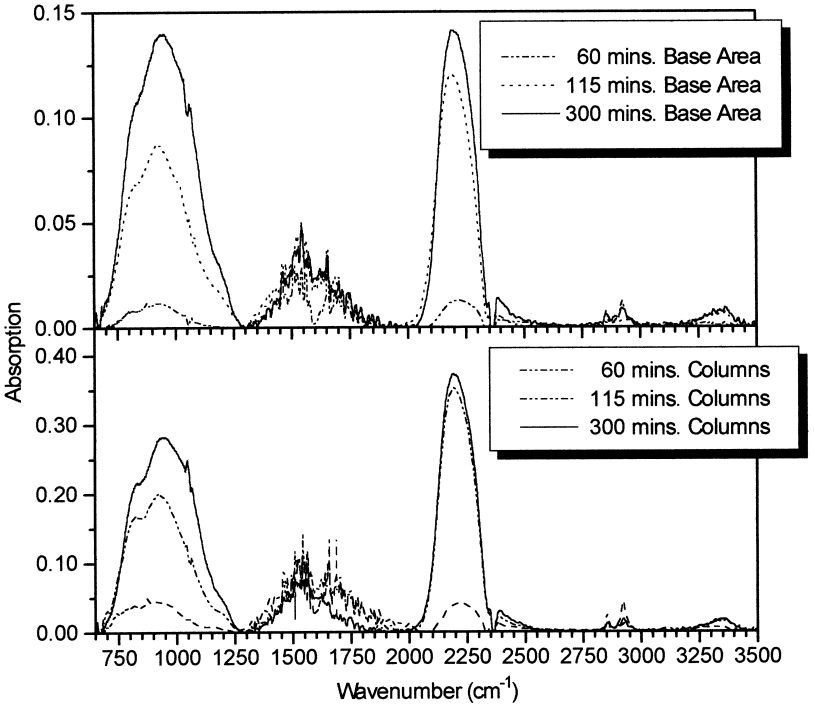

Fig. 5. Small-area FTIR spectra of the column and base areas of samples prepared at different deposition times.

atom such that the vibration becomes more symmetric. We observe that the 1200 cm^{-1} band moves to lower energies with bias and time, which is probably caused by a relaxation of the single C–N bond environment. Finally, the 800 cm^{-1} band shifts to higher energies with increased power and bias but remains practically unchanged versus deposition time. Since the frequency of the vibration od a pyramid structure is dependent on the cosine of the angle between the bonds and the direction of the displacement of the apex atom, any shift is more likely to be caused by a change in the angle than the nature of the bonds, since the elements involved do not change. Thus, the most favourable angle of the structure is probably determined by the bombardment, which in turn depends on the power and the bias.

We can see that the developed columns contain larger amounts of C and N, and in the base area, smaller columns grow continually. High plasma power favours the formation of or the transformation of C≡N to single, linear carbon–nitrogen bonds. Again, the dependence of the characteristics of the deposits on the bias is not completely clear and requires additional work, perhaps involving RF biasing to remove the complication of the inefficiency of DC biasing of an insulating substrate.

Raman spectra were taken on the material deposited on silicon substrates both from columns and non-columnar structures. In Fig. 7, spectra corresponding to columns of samples prepared under different bias are shown. Sometimes the photoluminescence (PL) masked the Raman signal. A first-order peak from the substrate can be seen in three of the samples, which implies that the material is transparent to laser light and its bandgap should be >1.96 eV. However, this poses a problem as to the interpretation of the spectra as it is difficult to identify whether the whole signal is coming from the columns, the interface or the substrate itself, especially as the spectra taken from the non-column areas were similar. At zero and -100 V bias, little or no PL can be observed: at -200 V it peaks within the range under study, and finally the luminescence band shifts to higher energies when the applied voltage is set to -300 V, although under the experimental conditions its maximum could not be observed. This signal could originate from the interface, where damaged silicon is produced, as demonstrated by the broad feature around the first-order Si Raman peak. On the other hand, when the sample prepared using 600 W of RF power and a bias of -200 V was illuminated with ultraviolet radiation (250 nm), yellow light could be observed by the naked eye, so extreme conditions give place to changes in the electro-optical properties of the films.

In the Raman spectra, the G and D bands of disordered graphite are detected at $\sim$1600 and 1360 cm^{-1}, respectively, and appear in all samples, indicating that there is a graphitic phase present within and/or below the columns. Apart from the sample prepared under no applied bias, no distinct features are seen in the spectra, with the exception of those related to the silicon substrate. The peaks observed in the spectrum of the sample

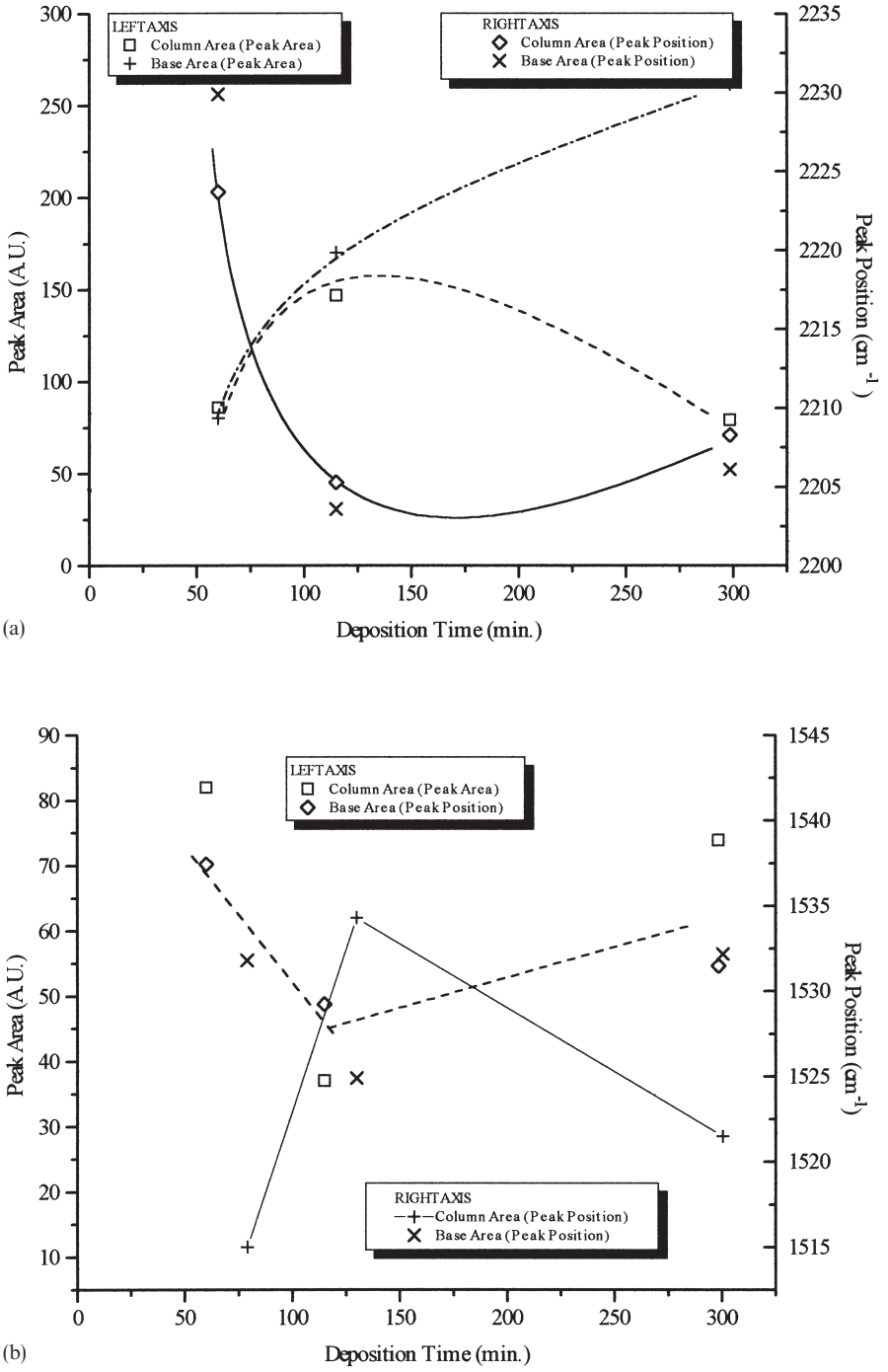

Fig. 6. (a) Variation of the area and position of the 2200 cm^{-1} of the FTIR spectra as a function of deposition time. (b) Variation of the area and position of the 1200 cm^{-1} of the FTIR spectra as a function of deposition time.

deposited using no external bias were only observed in columnar structures, but as yet we have not been able to identify them with precise vibrational modes, except for a small pouch between 600 and 700 cm^{-1} which has been observed in sputtered CN films [29], and a mode of β-C_3N_4 has also been predicted and reported to appear in that region [10]. There are clear differences between the Raman and the IR spectra: given that the Raman modes in graphitic CN become active in IR [23], it is possible to say that the IR peaks at 830, 1000, 1200 and 2200 cm^{-1} are not from graphitic rings since they are not Raman-active. It is worth noting that although the nitrile stretching mode appears as a strong absorption peak in the IR spectra at ~2200 cm^{-1}, it is difficult to detect it in the Raman spectra. Other authors who have reported IR and Raman spectra of CN films

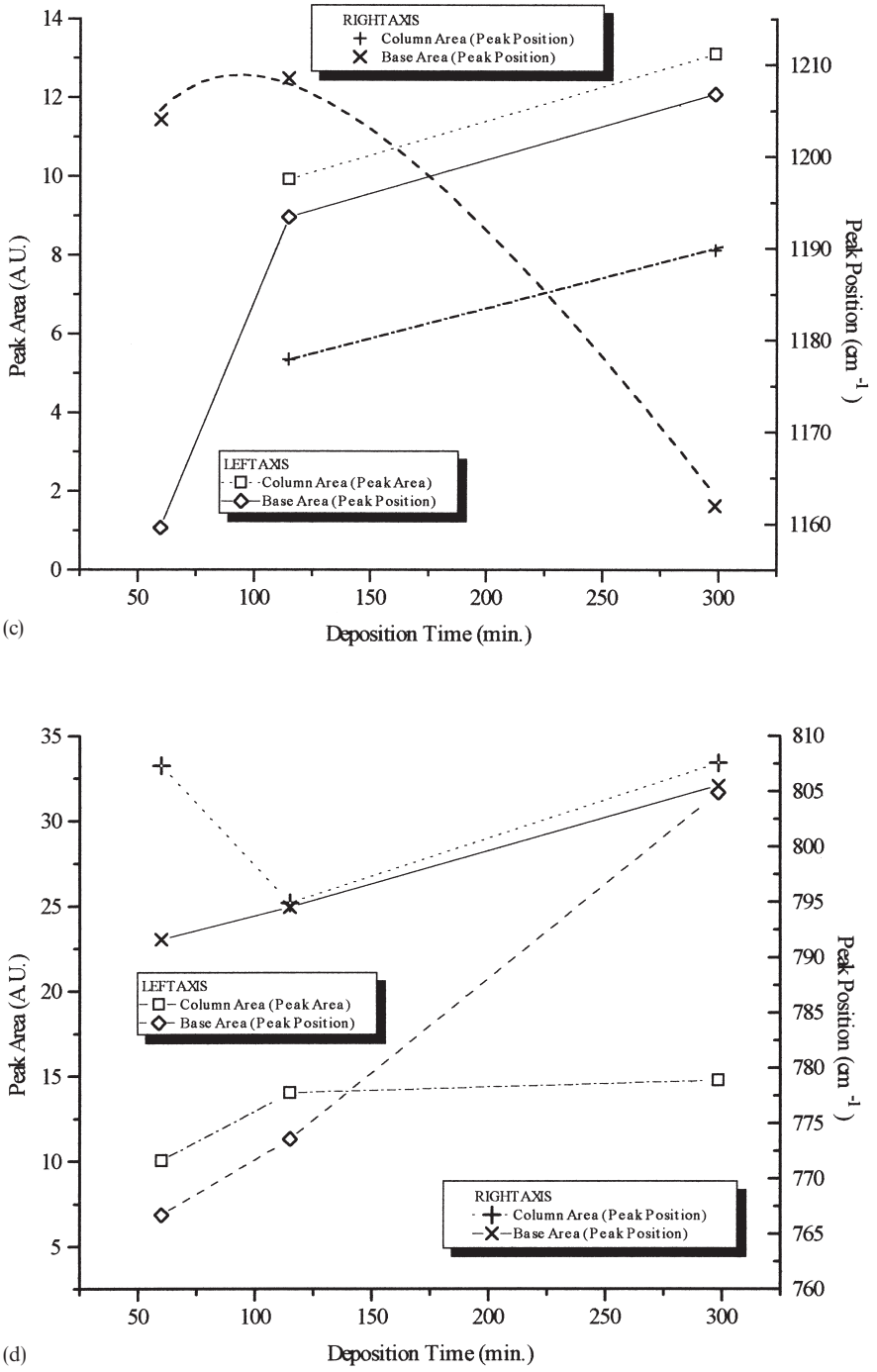

Fig. 6. (c) Variation of the area and position of the 1500 cm^{-1} of the FTIR spectra as a function of deposition time. (d) Variation of the area and position of the 800 cm^{-1} of the FTIR spectra as a function of deposition time.

have described a similar situation: this could be due to symmetry restrictions.

Finally, it should be noted that the deposits were found to be stable to the application of the 20 keV electron beam used in the SEM work, and no change was observed in the IR spectra for samples annealed under vacuum up to 700 °C for 1 h.

4. Conclusions

Deposits containing carbon and nitrogen in amounts equal to the stoichiometric value of C_3N_4 have been prepared by a high power-density hollow-cathode plasma-assisted method which involves both chemical and physical sputtering of a graphite target by nitrogen.

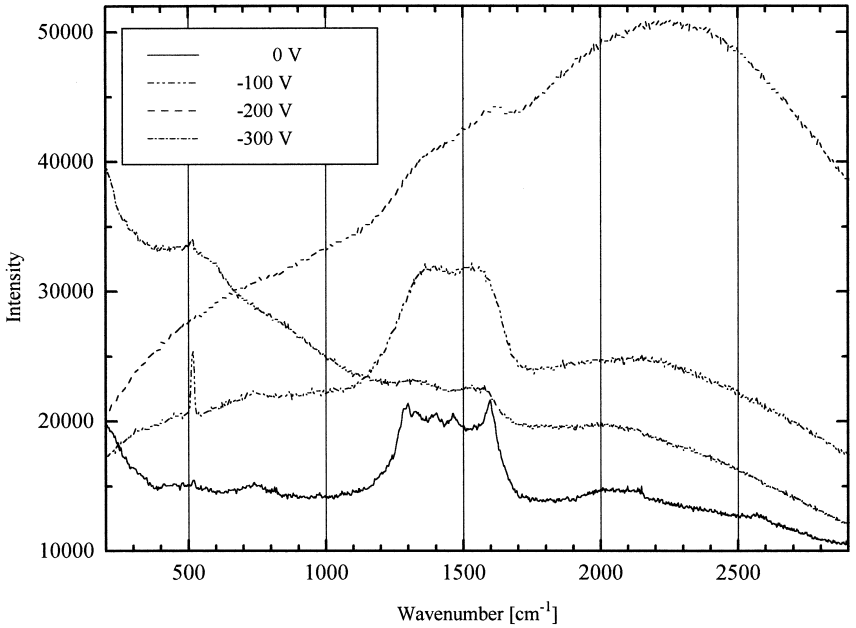

Fig. 7. Raman spectra of four samples prepared under different subastrate bias, using 500 W of RF power and the optimal conditions indicated in Table 1. Bands related to disordered carbon are seen in all spectra.

The addition of small amounts of methane in the gas mixture was found to enhance the deposition rate without causing significant inclusion of either CH or NH groups. Plasma probe measurements showed that the electron temperature of the plasma produced with this hollow-cathode reactor in the substrate region under optimum conditions is remarkably high. The deposits show a columnar structure, of dimensions of up to ~20 mm in diameter and 15 mm high. The observed cone shape of the columns is very similar to that seen in other deposits, where bombardment of the coating plays a definitive role [30]. Transmission and X-ray diffraction showed that the material is at least partially polycrystalline. At present it is not possible to establish which crystal structure or structures are formed. Our IR spectra are somewhat different to most spectra which have been reported for this material (although most of the other reports did not deal with stoichiometric CN). This implies that our material has a distinct bonding configuration and possibly a different structure. The deposits were stable under vacuum up to 700 °C.

Acknowledgement

We thank Jose Guzman, Ernesto Sanchez, Leticio Baños, Dr. Enrique Sansores and Dr. Enrique Camps for their help with electron microscopy, small-area FTIR, X-ray diffraction studies, theoretical X-ray data calculations and plasma probe analysis, respectively. We also acknowledge the financial support of CONACyT, DGAPA and the European Union through projects 3333-A9308, IN105094 and C11*-CT93-0039 (DG12 HMSU). A.G. also acknowledges CONACyT for a postgraduate scholarship (93447).

References

[1] M.L. Cohen, Phys. Rev. B 32 (1985) 7988.
[2] M.L. Cohen, Nature (London) 388 (1989) 291.
[3] A.Y. Liu, M.L. Cohen, Science 245 (1989) 841.
[4] A.Y. Liu, M.L. Cohen, Phys. Rev. B 41 (1990) 10727.
[5] M.Y. Chen, X. Lin, V.P. Dravid, Y.W. Chung, M.S. Wong, W.D. Sproul, Surf. Coat. Technol. 5455 (1992) 360–364.
[6] X.A. Zhao, C.W. Wong, Y.C. Tsang, Y.W. Wong, P.W. Chan, C.L. Choy, Appl. Phys. Lett 66 (1995) 2652–2654.
[7] L. Maya, D.R. Cole, E.W. Hagarman, J. Am. Ceram. Soc. 74 (1991) 1686–1688.
[8] M. Diani, A. Mansour, L. Kubler, J.L. Bischoff, D. Bolmont, Diamond Relat. Mater. 3 (1994) 264–269.
[9] A. Hoffman, I. Gouzman, R. Brener, Appl. Phys. Lett. 64 (1994) 845.
[10] T.Y. Yen, C.P. Chou, Appl. Phys. Lett. 67 (1995) 2801.
[11] Z.J. Zhang, S. Fan, C.M. Lieber, Appl. Phys. Lett. 66 (1995) 3582–3584.
[12] L.R. Doolittle, Nucl. Instrum. Methods Phys. Res. 15 (1986) 227.
[13] D.R. Lide (Ed.), CRC Handbook of Chemistry and Physics, 76th ed. CRC Press, Boca Raton, FL, 1995.
[14] S.F. Durrant, E.C. Rangel, M.A. Bica de Moraes, J. Vacuum Sci. Technol. A 13 (1995) 1901.
[15] K.J. Clay, S.P. Speakman, G.A.J. Amaratunga, S.R.P. Silva, J. Appl. Phys. 79 (1996) 7227.
[16] Y. Zhang, Z. Zhou, H. Li, Appl. Phys. Lett. 68 (1996) 634.
[17] D.M. Teter, R.J. Hemley, Science 271 (1996) 53.

[18] J. Szmidt, A. Werbowy, K. Zdunek, A. Sokowska, J. Konwerka-Hrabouska, S. Mitura, Diamond Relat. Mater. 5 (1996) 564.
[19] L.C. Chen, C.Y. Yang, D.M. Bhousari, K.H. Chen, M.C. Lin, J.C. Lin, T.J. Chuang, Diamond Relat. Mater. 5 (1996) 514.
[20] K.M. Yu, M.L. Cohen, E.E. Haller, W.L. Hansen, A.Y. Liu, I.C. Wu, Phys. Rev. B 49 (1994) 5034.
[21] D. Li, E. Cutiongco, Y.W. Chung, M.S. Wong, W.D. Sproul, Surf. Coat. Technol. 6869 (1994) 611.
[22] C.W. Ong, X.A. Zhao, Y.C. Tsang, C.L. Choy, P.W. Chan, Thin Solid Films 280 (1996) 1.
[23] J.H. Kauffman, S. Metin, D.D. Saperstein, Phys. Rev. B 39 (1989) 13053.
[24] A. Bousetta, M. Lu, A. Bensaoula, A. Schultz, Appl. Phys. Lett 65 (1994) 696.
[25] N.B. Colthup, L.H Daly, S.E. Wiberley, Introduction to Infrared and Raman Spectroscopy, 2nd ed., Academic Press, New York, 1975, p. 54.
[26] S. Veprek, J. Weidemann, F. Glatz, J. Vacuum Sci. Technol. A 13 (1995) 2914.
[27] J. van Der Maas, T. Visser, in: H.A. Willis, J. Van der Maas, R.G.J. Miller (Eds.), Laboratory Methods in Vibrational Spectroscopy, Wiley, Chichester, 1987, pp. 25–43.
[28] J. Widany, F. Weich, Th. Köhler, D. Porezag, Th. Fruenheim, Diamond Relat. Mater. 5 (1996) 1031.
[29] J. Koskinen, J.P. Hirvonen, J. Levoska, P. Torri, Diamond Relat. Mater. 5 (1996) 669.
[30] R. Messier, personal communication.